Optical-microphysical cirrus model

J. Reichardt,[1,2] S. Reichardt,[1] R.-F. Lin,[3,4] M. Hess,[5] T. J. McGee,[6] and D. O. Starr[4]

Received 5 March 2008; revised 15 July 2008; accepted 4 August 2008; published 18 November 2008.

[1] A model is presented that permits the simulation of the optical properties of cirrus clouds as measured with depolarization Raman lidars. It comprises a one-dimensional cirrus model with explicit microphysics and an optical module that transforms the microphysical model output to cloud and particle optical properties. The optical model takes into account scattering by randomly oriented or horizontally aligned planar and columnar monocrystals and polycrystals. Key cloud properties such as the fraction of plate-like particles and the number of basic crystals per polycrystal are parameterized in terms of the ambient temperature, the nucleation temperature, or the mass of the particles. The optical-microphysical model is used to simulate the lidar measurement of a synoptically forced cirrostratus in a first case study. It turns out that a cirrus cloud consisting of only monocrystals in random orientation is too simple a model scenario to explain the observations. However, good agreement between simulation and observation is reached when the formation of polycrystals or the horizontal alignment of monocrystals is permitted. Moreover, the model results show that plate fraction and morphological complexity are best parameterized in terms of particle mass, or ambient temperature which indicates that the ambient conditions affect cirrus optical properties more than those during particle formation. Furthermore, the modeled profiles of particle shape and size are in excellent agreement with in situ and laboratory studies, i.e., (partly oriented) polycrystalline particles with mainly planar basic crystals in the cloud bottom layer, and monocrystals above, with the fraction of columns increasing and the shape and size of the particles changing from large thin plates and long columns to small, more isometric crystals from cloud center to top. The findings of this case study corroborate the microphysical interpretation of cirrus measurements with lidar as suggested previously.

Citation: Reichardt, J., S. Reichardt, R.-F. Lin, M. Hess, T. J. McGee, and D. O. Starr (2008), Optical-microphysical cirrus model, *J. Geophys. Res.*, *113*, D22201, doi:10.1029/2008JD010071.

1. Introduction

[2] Extraction of microphysical information from lidar observations of cirrus clouds is a challenging scientific objective because for an ensemble of ice particles no straightforward relationship exists between the optical properties at the relevant backscattering direction and the microphysical properties. Recently, *Reichardt et al.* [2002c] reported lidar measurements of Arctic cirrus clouds which showed that (1) the particle optical properties, specifically depolarization ratio δ_{par} and extinction-to-backscatter ratio, or lidar ratio, S_{par}, were strongly correlated; (2) over the length of each cirrus measurement, the particle properties varied systematically; and (3) the particle optical properties depended on the ambient temperature. On the basis of theoretical particle optical data, these measurements were explained in terms of size, shape and growth of the cirrus particles. According to the interpretation of *Reichardt et al.* [2002c], light scattering by small hexagonal columns with aspect ratios close to one was dominant near the cloud top in the early stage of the cirrus development. Over time, as the cloud base extended to lower altitudes with warmer temperatures, the ice particles grew larger and became morphologically diverse: the optical lidar signature was indicative of a mixture of column- and plate-like particles (particles that have the scattering properties of hexagonal columns or plates, respectively). Toward the cloud base, light scattering was predominantly by plate-like ice particles. The proposed interpretation would hold out the prospect of model-supported retrieval of cirrus particle size, morphology (shape), and ice water content if it were

[1]Joint Center for Earth Systems Technology, University of Maryland, Baltimore County, Baltimore, Maryland, USA.
[2]Now at Meteorologisches Observatorium Lindenberg, Deutscher Wetterdienst, Tauche, Germany.
[3]Goddard Earth Sciences and Technology Center, University of Maryland, Baltimore County, Baltimore, Maryland, USA.
[4]Mesoscale Atmospheric Processes Branch, Laboratory for Atmospheres, NASA Goddard Space Flight Center, Greenbelt, Maryland, USA.
[5]Remote Sensing Technology Institute, German Aerospace Center, Wessling, Germany.
[6]Atmospheric Chemistry and Dynamics Branch, Laboratory for Atmospheres, NASA Goddard Space Flight Center, Greenbelt, Maryland, USA.

Copyright 2008 by the American Geophysical Union.
0148-0227/08/2008JD010071

validated. In this follow-up article we test the findings of *Reichardt et al.* [2002c] for their applicability to cirrus remote sensing.

[3] The direct approach to testing the newly developed retrieval method would be to check the retrieval results against in situ measurements (as it was done by, e.g., *Intrieri et al.* [1993], *Donovan et al.* [2001] and *Benedetti et al.* [2003]), however, this is not possible in our case because cirrus sampling was not performed during the lidar measurements. Therefore we pursue a different line of approach: A cirrus model with explicit microphysics [*Lin et al.*, 2005] is employed to simulate the geometrical evolution of the ice cloud, the microphysical data are then converted to cirrus optical properties on the basis of the interpretation of *Reichardt et al.* [2002c], and finally synthetic optical data and lidar observations are compared.

[4] The optical-microphysical model developed for this study differs from other cirrus models in output and scope. To the best of our knowledge, it is the first model that simulates depolarization ratio and lidar ratio measurements with lidar. Previous cirrus investigations focused on making available optical and radiative properties that are relevant to radiative transfer calculations, and thus optical schemes were implemented that estimated cloud properties such as particle extinction and absorption coefficients, single scattering albedo, asymmetry parameter and ice water content, but not δ_{par} and S_{par} [*Mitchell and Arnott*, 1994; *Mitchell et al.*, 1996b; *Westphal et al.*, 1996; *Khvorostyanov and Sassen*, 1998; *Harrington and Olsson*, 2001; *Liu et al.*, 2003]. The optical-microphysical model is employed to investigate the credibility of assumptions made about the relationship between optical and microphysical properties of cirrus clouds, while most other cirrus modeling efforts utilize remote or in situ measurements to validate the cloud model, and to refine model parameters [e.g., *Jensen et al.*, 1994; *Mitchell*, 1994; *Mitchell et al.*, 1996a; *Westphal et al.*, 1996; *Chen et al.*, 1997; *Fouilloux and Iaquinta*, 1998; *Benedetti and Stephens*, 2001; *Khvorostyanov et al.*, 2001, 2003]. Probably closest to our approach is the one followed by *Sassen et al.* [2002] where a cirrus model with explicit microphysics is used to test empirical relationships between ice water content and radar reflectivity.

[5] Certainly, the analysis presented in this study cannot be regarded as a substitute for field campaigns combining remote and in situ observations [*Whiteway et al.*, 2004], because a self-consistent model description of cirrus measurements with lidar does not necessarily mean the underlying interpretation given by *Reichardt et al.* [2002c] is correct. But it is useful to test whether it is plausible, to define parameter spaces, to point at deficiencies, and, if convincing agreement is achieved, to support the basic concept.

[6] The article is organized as follows: In section 2 a description of the optical-microphysical model is presented. In section 3 the functional relationships between optical and microphysical properties are developed, and the various model parameters are defined. Particle morphological complexity and particle preferred orientation are taken into account, which have not been included previously [*Reichardt et al.*, 2002a]. The optical-microphysical model is then applied to the measurement case of an Arctic cirrus cloud in a first case study (section 4). In the discussion emphasis is put on the intercomparison of modeled and measured optical properties. The sensitivity tests that were performed to correctly reproduce the spatial and temporal evolution of the ice cloud are only briefly discussed as these are the objective of a companion paper [*Lin et al.*, 2005]. Section 5 is a summary and outlook.

2. Optical-Microphysical Model

[7] Figure 1 is a schematic of the coupled optical and microphysical cirrus model. In two independent iterative processes the lidar measurements are used to optimize cloud modeling. In a first process cirrus microphysics are simulated as a function of height and time. Meteorological data that are input to the microphysical model are profiles of temperature, humidity, and vertical wind velocity. A first guess is derived from radiosonde and wind profiler measurements concurrent with the lidar observation, or from mesoscale simulations (when available). The nucleation scheme is prescribed. Humidity, vertical wind velocity, and nucleation parameters are then deduced from sensitivity tests where the values selected yield the best agreement between (1) the observed and modeled temporal evolution of the cirrus cloud system (cloud height and vertical extent) and (2) the observed and modeled particle extinction profile.

[8] The time- and height-resolved microphysical data are then input to the optical model used for simulating the cirrus cloud as monitored with lidar. The particle size distributions are converted to cloud optical properties (including the lidar ratio and the depolarization ratio) by use of theoretical optical data obtained by ray-tracing computations. Different model scenarios, and thus sets of model parameters, can be selected to study the dependence of the relationship between cloud optical and microphysical properties on the assumptions made about the (size- and temperature-dependent) morphology and spatial orientation of the ice particles. Optimum model scenario and parameters are found by comparison between observed and modeled cirrus particle optical properties. Features of the microphysical model that were developed specifically for the purpose of coupled optical and microphysical modeling of cirrus clouds are summarized in section 2.1. A description of the optical model is given in section 2.2.

2.1. Microphysical Model

[9] The cirrus model used is the one-dimensional (spatial) version of the model of *Lin* [1997; see also *Lin et al.*, 2005]. The size distributions of ice particles (in terms of particle mass) are explicitly resolved and their evolution due to diffusional growth, aggregation, and differential sedimentation is explicitly simulated. A limitation of the model is that the principal shape of the cirrus crystals needs to be preselected. Furthermore, only hexagonal columns or plates can be chosen although it is known that microphysical processes exhibit a dependence on particle morphology. Our sensitivity tests with regard to morphology show, however, that generally results obtained for the two particle shapes available do not differ significantly in both integrated and mass-resolved parameters (as demonstrated by the intercomparison presented in Figure 2). For this reason, we perform our cirrus simulations under the assumption of columnar particle habit, and consider the microphysical model results as representative for ice particles of all shapes.

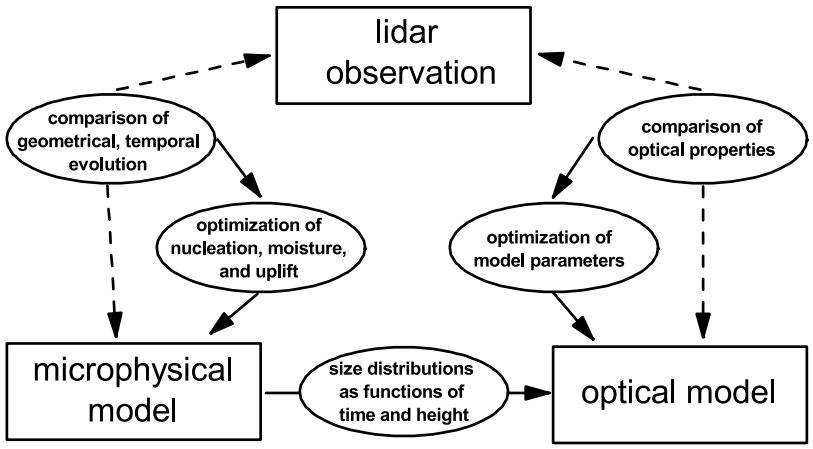

Figure 1. Schematic of the optical-microphysical model. Dashed arrows indicate comparisons between the observations and the two model modules which are used to optimize model parameters. Solid arrows indicate flow of data.

[10] Experiments confirm that under controlled laboratory conditions the shape of ice particles depend on the nucleation temperature (and the supersaturation [see, e.g., *Mason et al.*, 1963; *Bailey and Hallett*, 2004]). As will be discussed in more detail in section 3, a dependence of particle morphology on height, and thus temperature, is also observed in natural cirrus clouds albeit not always and less pronounced. In order to have the nucleation temperature available as a possible parameter in our optical simulation, we modified the microphysical model to keep track of the nucleation temperatures of the ice particles. Model output now includes the nucleation temperature distribution of the cirrus particles for each mass bin at each height grid box.

[11] Nucleation temperature is resolved in 0.7° intervals between −73.0 and −24.8°C. Particle mass spectra are registered in 40 mass bins between 3×10^{-15} and 2×10^{-5} kg, the bin width increases exponentially. Both homogeneous freezing of solution droplets and deposition nucleation [*Meyers et al.*, 1992] are taken into account.

2.2. Optical Model

[12] The optical model combines the cloud microphysical simulation with theoretical optical data of ice particles to provide synthetic cirrus profiles for the comparison with the lidar observations.

2.2.1. Basic Equations

[13] As explained in our previous publications [*Reichardt et al.*, 2002b, 2002c, 2002d], the optical properties that do not depend on the particle number density are particularly important in cirrus investigations, these are the lidar ratio

$$S_{\mathrm{par}} = \alpha_{\mathrm{par}}/\beta_{\mathrm{par}}, \tag{1}$$

i.e., the ratio of particle extinction coefficient α_{par} to backscatter coefficient β_{par}, and the particle linear depolarization ratio

$$\delta_{\mathrm{par}} = \beta^{\perp}_{\mathrm{par}}/\beta^{\parallel}_{\mathrm{par}}. \tag{2}$$

In equation (2), $\beta^{\perp}_{\mathrm{par}}$ and $\beta^{\parallel}_{\mathrm{par}}$ are the backscatter coefficients in the polarization planes orthogonal and parallel, respectively, to the linearly polarized lidar radiation source.

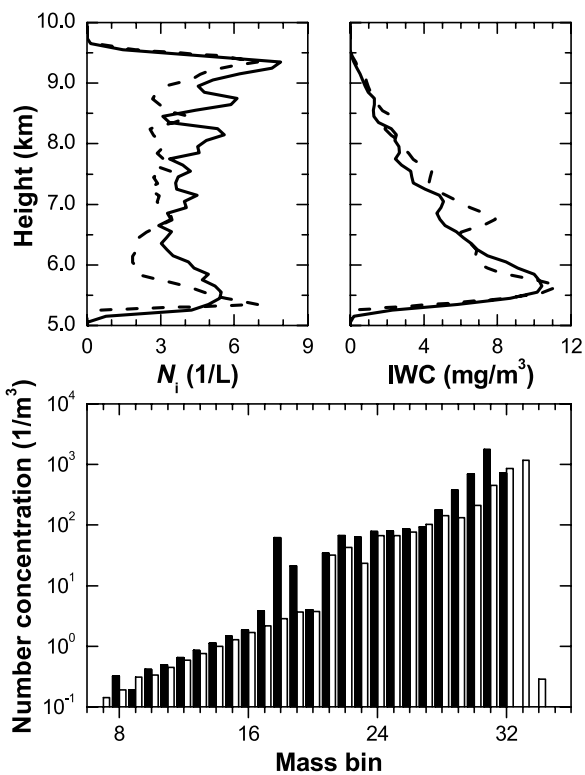

Figure 2. (top left) Integrated particle number concentration N_i and (top right) ice water content IWC for microphysical model runs with exclusively hexagonal columns (solid curves) or plates (dashed curves). Initialization of the model is for the 16 January 1997 cirrus case study presented in section 4. The simulation time is 300 min. (bottom) Mass-resolved particle number concentration for columns (solid bars) and plates (open bars) at a height of 7.5 km. Data are shown with a vertical resolution of 100 m.

[14] Similarly to the approach discussed in detail by *Reichardt et al.* [2002d], simulated extinction coefficient and backscatter coefficients, and thus S_{par} and δ_{par}, are calculated according to

$$\alpha_{\mathrm{par}} = 2\sum_{i,j,k} G_k(m_j) f_k(m_j, T_{\mathrm{n},i}) n(m_j, T_{\mathrm{n},i}), \tag{3}$$

$$\beta_{\mathrm{par}} = 2\sum_{i,j,k} p_k^{\pi}(m_j, T_{\mathrm{n},i}) G_k(m_j) f_k(m_j, T_{\mathrm{n},i}) n(m_j, T_{\mathrm{n},i}), \tag{4}$$

$$\beta_{\mathrm{par}}^{\perp} = 2\sum_{i,j,k}\left[\frac{\Delta_k(m_j, T_{\mathrm{n},i})}{1+\Delta_k(m_j, T_{\mathrm{n},i})} p_k^{\pi}(m_j, T_{\mathrm{n},i}) G_k(m_j) \times f_k(m_j, T_{\mathrm{n},i}) n(m_j, T_{\mathrm{n},i})\right], \tag{5}$$

$$\beta_{\mathrm{par}}^{\parallel} = 2\sum_{i,j,k}\left[\frac{1}{1+\Delta_k(m_j, T_{\mathrm{n},i})} p_k^{\pi}(m_j, T_{\mathrm{n},i}) G_k(m_j) \times f_k(m_j, T_{\mathrm{n},i}) n(m_j, T_{\mathrm{n},i})\right]. \tag{6}$$

The coefficients are sums over the spectrum of the particle mass m_j, $j = 1\ldots40$, the spectrum of the particle nucleation temperature $T_{\mathrm{n},i}$, $i = 1\ldots70$, and over the fractions f_k of the various particle types considered in this study [$\sum_k f_k(m_j, T_{\mathrm{n},i}) = 1$ for all m_j and $T_{\mathrm{n},i}$]. Specifically, these are randomly oriented hexagonal columns (f_1) and plates (f_2), and horizontally aligned hexagonal columns (f_3) and plates (f_4). Mass and nucleation temperature spectra, and the particle number density n are output of the microphysical model runs.

[15] p^{π} and Δ denote, respectively, the value of the scattering phase function and the linear depolarization ratio at the lidar-relevant backscattering direction, and are taken from a database of theoretical particle optical properties (see section 2.2.2). The efficiency of scattering of light in the visible spectrum by cirrus particles is equal to 2. The geometrical cross section G is a function of particle morphology and particle orientation. For particles with hexagonal symmetry we find for plates

$$G = \frac{3}{16}\sqrt{3}\frac{d^2}{A^2}(1+\cos\omega_{\mathrm{m}}) + \frac{3}{2\pi}\frac{d^2}{A}\frac{\omega_{\mathrm{m}} - \sin\omega_{\mathrm{m}}\cos\omega_{\mathrm{m}}}{1-\cos\omega_{\mathrm{m}}}, \tag{7}$$

and for columns

$$G = \frac{3}{16}\sqrt{3}\frac{d^2}{A^2}\sin\omega_{\mathrm{m}} + \frac{3}{2\pi}\frac{d^2}{A}\frac{\omega_{\mathrm{m}} + \sin\omega_{\mathrm{m}}\cos\omega_{\mathrm{m}}}{\sin\omega_{\mathrm{m}}}, \tag{8}$$

where d is the maximum dimension of the particle, A its length-to-diameter ratio (aspect ratio), and ω_{m} is the maximum value of the angle ω the particle is permitted to wobble about the horizontal plane. Because ω is uniformly distributed, $\omega_{\mathrm{m}} = \pi/2$ corresponds with an ensemble of identical hexagons in random (3-D) orientation whereas $\omega_{\mathrm{m}} = 0$ describes the case of perfect horizontal particle alignment (2-D orientation).

2.2.2. Theoretical Optical Data

[16] As will be detailed in section 3.1, ice particles of natural cirrus clouds (except for cirrus anvils) are often simple, pristine hexagonal crystals (columns, plates) or aggregates of hexagonal crystals (e.g., capped columns, bullet rosettes), with aspect ratio depending on crystal size and shape perfection depending on atmospheric conditions. (Possibly the mechanism of aggregation is not strong enough to explain the observations of aggregates, and these particles form instead through growth of plate and/or column features over their life cycle during which they experienced a spectrum of temperature and supersaturation conditions. So aggregate-appearing particles could be a better term.) In order to account for these particles in our model, we employ theoretical optical data determined for the two optically distinct classes of hexagonal columns and plates, and assume that a composite particle scatters similarly to the ensemble of basic crystals that formed it [*Macke*, 1993; *Iaquinta et al.*, 1995; *Yang and Liou*, 1998].

[17] Furthermore, the orientation of the ice particles is an issue that has to be addressed (see the discussion by *Reichardt et al.* [2002c]). Falling ice particles larger than a critical size have the tendency to assume an orientation with their maximum geometrical dimension in the horizontal plane (2-D orientation). If the crystal faces of these 2-D-oriented particles are aligned horizontally, their optical properties as observed with lidar deviate significantly from those found for random (3-D) orientation because of specular reflections. Since this is likely the case of crystals with aspect ratios $\ll 1$, observations of very low depolarization ratios [e.g., *Platt et al.*, 1978; *Reichardt et al.*, 2002c] and lidar ratios [*Ansmann et al.*, 1992; *Reichardt et al.*, 2002c] are often attributed to the existence of 2-D-oriented hexagonal plates. On the other hand, the dependence of the optical properties of columnar hexagons and aggregates on orientation may be less pronounced, or different, because of probable rotations about the center axis and intrinsic randomness, respectively. Thus analysis of the optical properties of particles with reduced orientational freedom is part of our studies.

[18] We applied the ray-tracing technique to calculate the optical data of hexagonal columns and plates for different degrees of orientational freedom (16 ω_{m} values between 0 an $\pi/2$). Pure ice without particulate inclusions was assumed as is suggested by the studies of *Seifert et al.* [2003]. To better describe scattering from natural cirrus particles, optical properties of slightly distorted rather than perfect crystals were modeled [*Hess et al.*, 1998]. The artificial surface distortion was determined in sensitivity tests where the agreement between computational data and the upper and lower boundaries of the particle optical properties as measured by polarization Raman lidar in Arctic cirrus clouds was optimized [*Reichardt et al.*, 2002c]. Figure 3 illustrates the dependence of the lidar ratio and the depolarization ratio on the maximum wobble angle. A uniform ω distribution is assumed; results obtained with a normal distribution are basically the same. Ranges of optical data obtained for 3-D-oriented hexagons are given by the shaded areas in Figure 3 for comparison (compare Figure 4 [see also *Reichardt et al.*, 2002c]). With decreasing wobble angle, the plate optical properties decrease monotonously

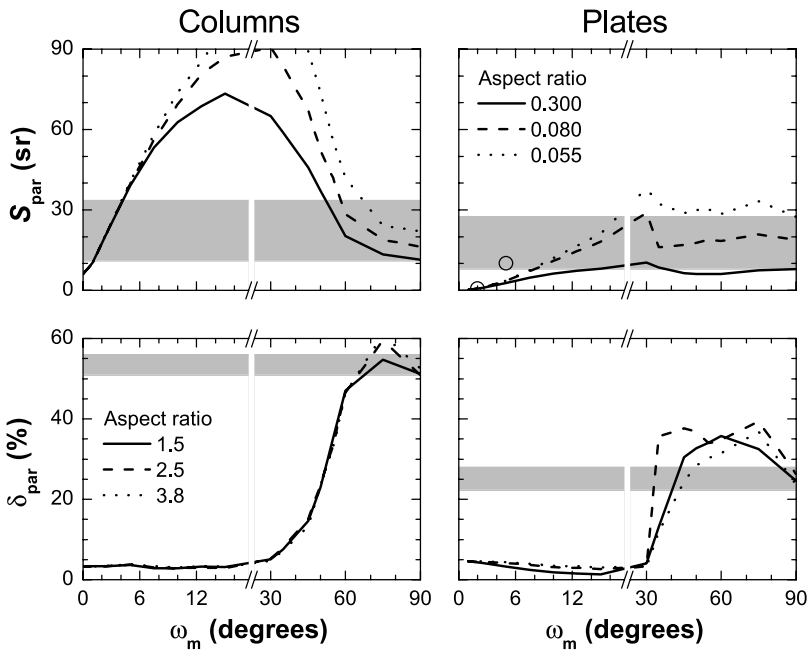

Figure 3. Lidar ratio S_{par} and depolarization ratio δ_{par} of horizontally aligned hexagonal ice particles as functions of maximum wobble angle ω_m for different aspect ratios. Because of a uniform angle distribution, $\omega_m = 90°$ is equivalent to random orientation. The data have been derived with geometrical-optics ray-tracing calculations [*Hess et al.*, 1998]. Crystal shapes are assumed to be slightly distorted; the distortions are assumed to be the same as those used for the computations of the optical properties of ice hexagons in random orientation [*Reichardt et al.*, 2002c], which are indicated by the shaded areas. Lidar ratios of cirrus clouds consisting of ice plates (open circles at maximum wobble angles of 2° and 5°) obtained with a physical-optics method by *Yang et al.* [2003] are given for comparison. Note the change of scale at $\omega_m = 18°$.

to very low values which is in agreement with earlier theoretical studies, and so does the column depolarization ratio. Remarkably, the lidar ratio of columns exhibits a different behavior. In this case, values are larger than the 3-D lidar ratio except for those of almost perfectly aligned crystals.

[19] From these findings the following important conclusions can be drawn. First, particle alignment is readily detectable with polarization measurements, even if the degree of orientation is not high. For $\omega_m < 35°$, δ_{par} values of aligned particles are always lower than those of crystals in random orientation. Second, particle orientation evades detection in S_{par} unless $\omega_m < 1°$ (columns), or $\omega_m < 8°$ (plates). For larger ω_m, alignment may even result in higher S_{par} than in the case of 3-D orientation. Third, because of the intrinsic disorder of aggregates, aligned polycrystals exhibit reduced δ_{par} and S_{par} only if a single crystal of the ensemble is optically dominant (i.e., is much larger) and if this crystal has a ω_m close to zero. Fourth, our computational results are similar for a wide range of aspect ratios (0.055–0.3), and should thus be valid for planar particles of all sizes (ray-tracing results do not depend on the assumed particle size if, as in our case, light absorption can be neglected, but aspect ratio and size of natural cirrus particles are loosely correlated, see section 3.3).

[20] The strength of these conclusions depend on the soundness and representativeness of our computations, particularly in view of the well-known limitations that apply to ray-tracing techniques. For crystals with slightly distorted surfaces, however, these methods may still be applicable, because crystal imperfections tend to smooth the features of the scattering phase matrix elements at lateral and backward scattering angles (see, e.g., *Macke et al.* [1996]), and computational results obtained for these particles prove to fit well to measurements. Furthermore, the study of *Yang et al.* [2003] lends confidence in using our ray-tracing results in our optical-microphysical cirrus model. Applying a physical-optics method, *Yang et al.* [2003] confirm the increase of lidar ratio with maximum wobble angle for cirrus clouds consisting of aligned planar crystals (Figure 3). The discrepancy between our geometrical-optics and the physical-optics S_{par} values at $\omega_m = 5°$ can be attributed to the assumption of a perfect planar habit by *Yang et al.* [2003].

3. Model Assumptions

[21] The general conception is outlined of how the distribution of the cloud particle population into the different particle types, and the translation of the microphysical into the optical properties of the ice particles is modeled, and the model parameters are defined.

3.1. Fractions of Particle Types

[22] Functions f_k are defined by the fraction of plates (f_{pla}), and by the fractions of horizontally oriented plates ($f_{2D,pla}$) and columns ($f_{2D,col}$):

$$f_1 = \left(1 - f_{2D,col}\right)\left(1 - f_{pla}\right), \tag{9}$$

$$f_2 = (1 - f_{2D,pla}) f_{pla}, \tag{10}$$

$$f_3 = f_{2D,col}(1 - f_{pla}), \tag{11}$$

$$f_4 = f_{2D,pla} f_{pla}. \tag{12}$$

Finding expressions for f_{pla}, $f_{2D,pla}$ and $f_{2D,col}$ is a difficult problem because not much is known about the complicated atmospheric processes that control particle shape, or that lead to the optical phenomena commonly attributed to the horizontal alignment of cirrus particles (see, e.g., the discussion by *Reichardt et al.* [2002c]). Therefore we examined in situ and remote observations to make reasonable assumptions about f_{pla}, $f_{2D,pla}$ and $f_{2D,col}$. Depending on the model scenario, they are prescribed as functions of different variables such as nucleation temperature, ambient temperature, and particle mass.

[23] According to laboratory experiments, ice crystals growing at temperatures $<-25°C$ should be principally of columnar shape while between $-8°C$ and $-25°C$ hexagonal plates are found [*Mason et al.*, 1963]. Furthermore, secondary growth features such as the needle-like extensions of columns or the fern-like development of star-shaped planar crystals occur only if the air is highly supersaturated relative to ice. However, under atmospheric conditions the dependence of particle habit on temperature is relaxed. In situ particle sampling suggests that a common, yet not general, vertical shape distribution of cold ($<\sim-25°C$) cirrus clouds is isometric crystals near the cloud top, relatively large monocrystals of imperfect hexagonal symmetry or simple bullet rosettes around the center of the ice cloud, and crystal clusters of arbitrary overall shape in the lower cirrus ranges [*Heymsfield and Iaquinta*, 2000; *Miloshevich et al.*, 2001; *Yang et al.*, 2001]. Planar crystals tend to be more numerous at warm temperatures [*Heymsfield and Platt*, 1984, and references therein], but are still present even at extremely cold temperatures [*Heymsfield*, 1986]. Following these observations we assume in our model that f_{pla} has the tendency to decrease from the base to the top of the cirrus cloud:

$$f_{pla} = \begin{cases} 1 + \tanh[h_1(X - h_2)] & : \quad X \le h_2, h_1 \ge 0 \\ 1 & : \quad X > h_2, \end{cases} \tag{13}$$

where X is either the ambient temperature T_a, the nucleation temperature T_n, or the particle mass m. Sensitivity tests have shown that function tanh simulates the anticipated dependence of f_{pla} on X well. Another advantage of this selection is that f_{pla} is controlled by only two model parameters, h_1 and h_2. For an illustration of f_{pla}, see Figures 10–12.

[24] Horizontal alignment of ice particles and its effect on the optical properties of cirrus clouds is a problem still not solved satisfactorily. It is not the intent of this paper to discuss this issue in detail, yet we give a brief justification of how we take particle orientation into account in our simulations. According to *Klett* [1995], all columnar and planar ice crystals larger $\sim$30 μm should be in 2-D orientation with averaged wobble angles small enough to effectively reduce δ_{par} (and probably S_{par}). If the particles occurring in natural cirrus clouds were predominantly pristine crystals, lidar measurements should show this characteristics most of the time. However, the multiyear cirrus statistics of the University of Utah Facility for Atmospheric Remote Sensing clearly demonstrates that particle orientation only has a weak effect on δ_{par}, particularly at temperatures $<-45°C$, at least at this midlatitude site [*Sassen and Benson*, 2001]. At these cold temperatures, on the other hand, large apparently flawless ice crystals of simple shape are not uncommon [see, e.g., *Yang et al.*, 2001] that should readily align in the horizontal plane and cause near-zero depolarization ratios. One way to reconcile theory with observations is the line of reasoning put forth by *Sassen* [1980] to explain the existence of halos. According to *Sassen* [1980], cirrus particles are mostly radiating groups of crystals rather than single crystals, and the individual crystal elements of such clusters can be considered to be randomly arrayed even though the composite particle may be horizontally aligned. Turbulence may add to the randomization of the particle orientation.

[25] In our model we adopt this view. We assume that the intrinsic disorder of 2-D-oriented polycrystals leads to optical properties that are similar to those of the ensemble of constituting basic crystals in random orientation, so that only 2-D-oriented monocrystals or 2-D-oriented clusters with a single, optically dominant scatterer (section 2.2.2) may show the optical signature of horizontally aligned particles. A consequence of this approach is that the fractions of (optically) aligned columns and plates, $f_{2D,col}$ and $f_{2D,pla}$, are usually small. Further, we assume that above a threshold size d_{2D} a fraction of c_{2D} particles experiences a decrease in orientational freedom (i.e., in ω_m) with size, with the gradient of the decrease being determined by parameter e_{2D}:

$$f_{2D} = c_{2D} \tag{14}$$

and

$$\omega_m = \begin{cases} \pi/2 \exp\left[-(d - d_{2D})^2/e_{2D}^2\right] & : \quad d \ge d_{2D} \\ \pi/2 & : \quad d < d_{2D}. \end{cases} \tag{15}$$

[26] Different parameter sets can be chosen for plates ($c_{2D,pla}$, $d_{2D,pla}$, $e_{2D,pla}$), and columns ($c_{2D,col}$, $d_{2D,col}$, $e_{2D,col}$).

3.2. Morphological Complexity

[27] The microphysical model assumes monocrystalline particles (hexagonal columns in our case). While it may be argued that this approximation is sufficient to simulate growth and sedimentation of agglomerated cirrus particles (despite the well-known habit dependence of virtually all microphysical processes), it is certainly not adequate to describe the optical properties of such crystal clusters. Particularly in the case of compact particle assemblages it is reasonable to assume that the constituting basic crystals possess less extreme aspect ratios than a single crystal with the same mass as the aggregate. Under the assumptions that the basic crystals scatter independently (as is the case of spatial particles with long protruding extensions) and show

Table 1. General Equations for Column and Plate Maximum Dimension d, Aspect Ratio A, and Ice Density ϱ[a]

Crystal Type	d (m)	A	ϱ (kg m^{-3})
Column, $m < 6.29 \times 10^{-12}$ kg	$0.1517\ (m/\mu)^{1/3}$	1.43	900
Column, 6.29×10^{-12} kg $< m < 2.55 \times 10^{-10}$ kg	$0.1987\ (m/\mu)^{0.3438}$	1.43	$345.47\ d^{-0.0915}$
Column, $m > 2.55 \times 10^{-10}$ kg	$\left(\frac{10^{8b_{\mathrm{col}}}}{109.73}\frac{m}{\mu}\right)^{1/(2.9085-2b_{\mathrm{col}})}$	$10^{\log\ 1.43+4b_{\mathrm{col}}}\ d^{b_{\mathrm{col}}}$	$345.47\ d^{-0.0915}$
Plate, $m < 9.34 \times 10^{-11}$ kg	$1.2459\ (m/\mu)^{0.4083}$	$1001.5^{-1}\ d^{-0.551}$	900
Plate, $m > 9.34 \times 10^{-11}$ kg	$\left(\frac{10^{-4b_{\mathrm{pla}}}}{93.531}\frac{m}{\mu}\right)^{1/(3+b_{\mathrm{pla}})}$	$10^{\log\ 0.16+4b_{\mathrm{pla}}}\ d^{b_{\mathrm{pla}}}$	900

[a] m is the mass of an individual particle, μ is the ratio of the particle mass as determined with the microphysical model to the mass of the optically active element, and b_{pla} and b_{col} are model parameters. The equations are a generalization of the parameterization by *Auer and Veal* [1970].

a narrow habit distribution, we can model the optical properties of morphologically complex particles by an optical break up of the crystal cluster. This is done by introducing function μ, $\mu \geq 1$, which is the ratio of the particle mass as determined with the microphysical model to the mass of the optically active element:

$$\mu = \begin{cases} \mu_0 + (\mu_0 - 1)\tanh[p_1(X - p_2)] & : \quad X \leq p_2, p_1 \geq 0 \\ \mu_0 & : \quad X > p_2. \end{cases} \tag{16}$$

[28] Either T_{a} or m can be substituted for X, but not T_{n}. We excluded this option because we consider it unlikely that the morphological complexity is governed by other than local variables. If $X = T_{\mathrm{n}}$ is chosen for modeling of f_{pla} (compare equation (13)), μ is still a function of T_{a}. The three model parameters μ_0, p_1 and p_2 apply to both columns and plates. The aspect ratio of the basic element, and hence S_{par} and δ_{par}, are then determined by $d(m/\mu)$ rather than by $d(m)$ (Table 1). The scattering cross section of a particle assemblage, however, is assumed to be better described by $G(m)$ than by $\mu\ G(m/\mu)$. Thus an increase in extinction coefficient upon optical break up is avoided. For an illustration of function μ, see Figure 11.

3.3. Relations Between Particle Size and Aspect Ratio

[29] The relation between the microphysical properties and δ_{par} and S_{par} of an ice particle is crucial to our model. Fortunately, two facts facilitate its parameterization. First, δ_{par} and S_{par} are determined by the shape of the particle, not its size, if absorption is negligible. For monocrystalline particles with hexagonal symmetry the parameter that controls these optical properties is the aspect ratio. Second, field studies show that in natural ice clouds aspect ratio and maximum dimension of particles of the same principal morphology are connected [*Ono*, 1969; *Auer and Veal*, 1970; *Heymsfield*, 1972; *Mitchell and Arnott*, 1994]. Generally, aspect ratios of columnar and planar particles, respectively, increase and decrease with size (thus optical properties indirectly depend on particle maximum dimension). Although the scatter in the individual data sets is quite large and a dependence on cirrus cloud type and season may exist, it is safe to say that the length-width relations of cirrus particles are comparatively well established.

[30] To allow for variability in the aspect ratio to size relationship of columns and plates, we generalized the parameterization of *Auer and Veal* [1970] for particles approximately larger than 100 μm by introducing the parameters b_{col} and b_{pla}. The general equations for maximum dimension d, aspect ratio A, and ice density ρ are summarized in Table 1 (particle mass is in kilograms). Note, that in our model m and function μ determine d, and thus A. In its turn, A determines S_{par} and δ_{par}.

[31] The effect of parameters b_{col} and b_{pla} on the aspect ratios of columns and plates is shown in Figure 4. Also shown are the theoretical optical properties used for particles in 3-D orientation [*Reichardt et al.*, 2002c]. Figure 4 illustrates that S_{par} is a sensitive indicator of particle size, whereas δ_{par} varies more with particle habit.

4. Application

[32] During January 1997 the GKSS Raman lidar [*Reichardt et al.*, 1996] was monitoring the winter atmosphere above the Esrange research station, Sweden (67.9°N, 21.1°E) in search for polar stratospheric clouds forming downwind the Scandinavian mountain ridge [e.g., *Reichardt et al.*, 2004]. This campaign provided the opportunity to collect a multiparameter data set of Arctic cirrus clouds, with the initial intention to compare it to the observations of midlatitude cirrus clouds made at the home base of the instrument near Geesthacht, Germany (53.5°N, 10.5°E) [*Reichardt*, 1999]. It was the discovery of a correlation among the particle optical properties of the Arctic cirrus clouds that sparked further investigations and led to a series of publications [*Reichardt et al.*, 2002b, 2002c; *Lin et al.*, 2005] of which this article is planned to be the final.

[33] For a first application of the optical-microphysical model the cirrus measurement taken on 16 January 1997 was selected, for it clearly shows the behavior summarized in section 1.

4.1. The 16 January 1997 Cirrus Cloud

[34] Operation of the lidar started at 1930 UT under favorable weather conditions. At 2010 UT a cirrus cloud began to move into the instrument field of view at around 8.8 km which could be observed for the next 7 h. The cloud event was associated with a surface warm front slowly moving over central Sweden and a strong northwesterly jet stream. Figure 5 illustrates the temporal evolution of the particle backscatter coefficient and the particle depolarization ratio of this long-lived cirrostratus, starting at 1945 UT to match the observation time with the simulation time of the microphysical model.

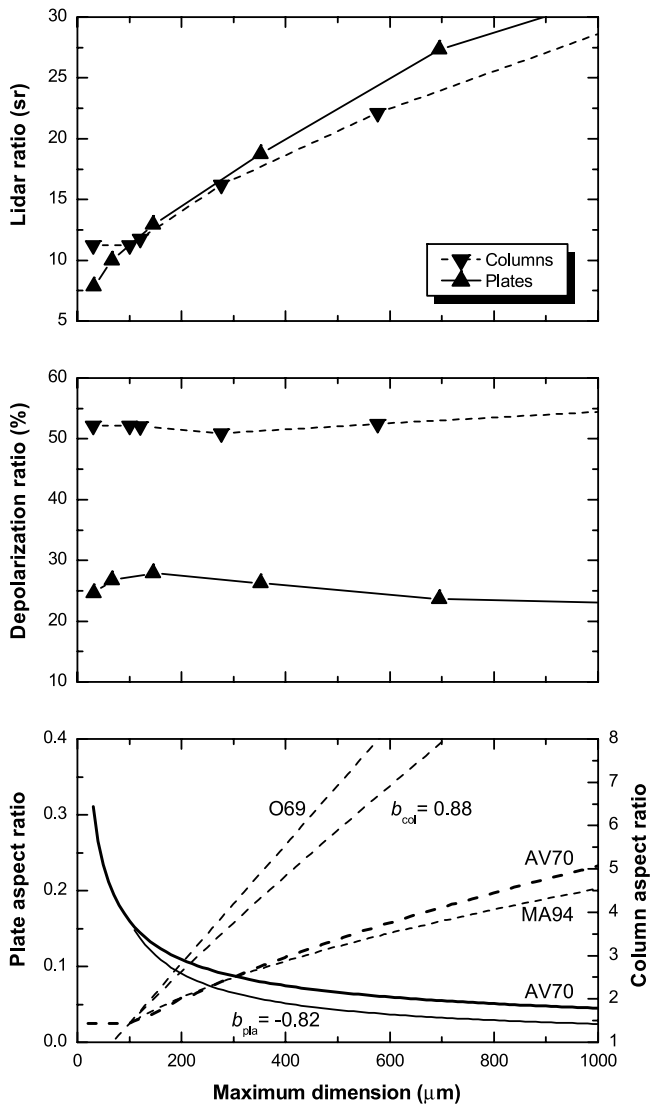

Figure 4. (top) Lidar ratio and (middle) depolarization ratio versus ice particle maximum dimension for solid hexagonal columns and plates in random orientation. Particle length-to-width (aspect ratio) relations of *Auer and Veal* [1970] and $\mu = 1$ are assumed. (bottom) Aspect ratio of hexagonal columns (dashed curves) and plates (solid curves) as a function of particle maximum dimension. Relations are plotted for $b_{col} = 0.88$ and $b_{pla} = -0.82$, which are the values used in this study (see section 4.4). Experimental results are shown for comparison (O69, $b_{col} = 0.98$ [*Ono*, 1969]; AV70, $b_{col} = 0.55$, $b_{pla} = -0.55$ [*Auer and Veal*, 1970]; MA94, $b_{col} = 0.50$ [*Mitchell and Arnott*, 1994]).

[35] Over time the cloud base lowered to approximately 4.3 km (−27.3°C) while the cloud top rose to about 10 km (−63.1°C). Generally, the backscatter coefficient (and the extinction coefficient) decreases, while the particle depolarization ratio increases, with cirrus altitude. Whereas many smaller-scale features are visible in the backscatter coefficient plot, the particle depolarization ratio is more homogeneous which indicates that this variability is mainly the effect of fluctuations in the particle number density (on which backscattering but not depolarization depends) and not in the particle properties themselves. Since the latter are the optical properties of interest here, specifically depolarization ratio δ_{par} and lidar ratio S_{par}, and these change slowly over time, we have not tried to simulate the small-scale features of the cirrus cloud in this study but focused on the overall development of the cirrostratus event.

[36] The determination of lidar ratios with Raman lidars requires relatively long integration times of lidar data to reduce the statistical errors to acceptable levels. Therefore we selected three time intervals for the S_{par} determination that exhibit little variability in cloud boundary heights and in the other number-density-independent optical property, δ_{par} (Figure 5). For a detailed description of the data evaluation process and an error analysis see *Reichardt et al.* [2002b], for a depiction of backscatter coefficient

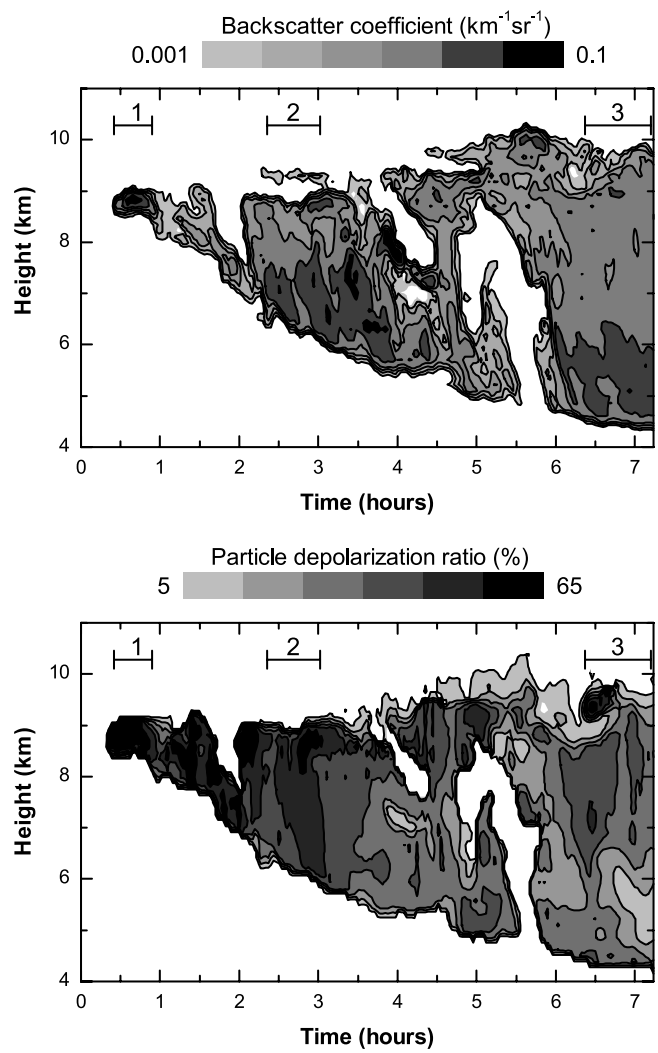

Figure 5. Height versus time display of (top) particle backscatter coefficient and (bottom) particle depolarization ratio generated from consecutive lidar profiles of the cirrus cloud measured on 16–17 January 1997 over northern Sweden. Three measurement intervals (bars) have been chosen for the comparison between observation and model. Time scale is the same for both measurement (starting at 1945 UT) and simulation.

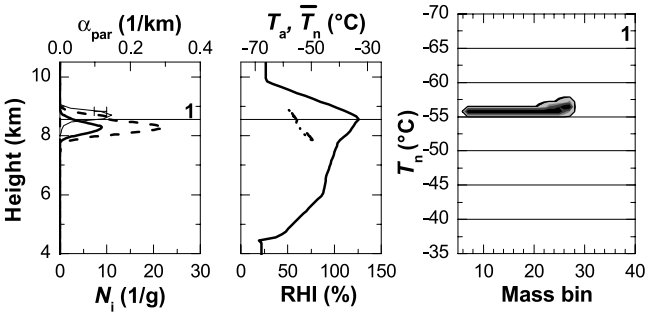

Figure 6. (left) Modeled extinction coefficient α_{par} (solid curve) and particle number concentration N_i (dashed curve) and (middle) relative humidity with respect to ice RHI (solid curve), mean nucleation temperature $\overline{T}_n$ (dotted curve, almost completely hidden behind the dashed curve) for interval 1, and ambient temperature T_a as measured with radiosonde (dashed curve). (right) Nucleation temperature (T_n) distribution (relative) as a function of particle mass for a selected height (height level marked in Figure 6 (left)). Black-rimmed white, light gray, gray, dark gray, and black areas indicate 0.005, 0.01, 0.1, 0.2, and 0.4 levels, respectively. Mass bins 5, 15, 25, and 35 correspond with particle maximum dimensions of 4, 17, 67, and 520 μm, respectively (column aspect ratios according to *Auer and Veal* [1970]). The lidar extinction measurement is shown for comparison (thin solid curve with statistical error bars (Figure 6, left)).

profiles, δ_{par} profiles, and S_{par} profiles for all three intervals see *Reichardt et al.* [2002c].

[37] The GKSS Raman lidar also measured profiles of water vapor. From these moisture data and from concurrent radiosonde temperature observations at Luleå (240 km south of Esrange) we retrieved estimates of relative humidity with respect to ice. However, the low absolute humidity over Esrange resulted in weak water vapor lidar signals that require long data integration times and restrict this analysis to altitudes <7 km, so in-cloud relative humidity is only available for interval 3 (see Figure 8).

4.2. Microphysical Simulation

[38] To initialize the microphysical model runs, radiosonde data of that night measured at the weather station of Luleå (65.6°N, 22.1°E) were used because local soundings were not available. Two tuning parameters were used to bring the simulated geometrical and temporal development of the cirrus cloud into agreement with the observations. These were the humidity profile for which the moisture data from the Luleå radiosonde served as a first guess, and the vertical wind speed which was assumed to be height- and time-independent ("synoptic forcing"). The tuning parameters were optimized over the course of a considerable number of sensitivity tests until a reasonable initial humidity profile and an optimum uplift of 2 cm/s were obtained. With lifting that weak, heterogeneous nucleation was the dominant nucleation mode, homogeneous nucleation did not become active. For all model runs, the vertical resolution in the model domain (3.8 to 10.8 km) was 20 m, the time step was 5 s for the advection terms and 0.1 s for particle growth.

[39] Figures 6–8 summarize the results of the microphysical simulations for intervals 1–3. Model data are integrated over the same time lengths as the lidar observations. To visualize the three-dimensional data sets, profiles of extinction coefficient, total ice particle number density and particle-spectrum-averaged nucleation temperature are shown together with the spectral nucleation temperature distribution of particles in a mass bin for selected cloud heights. Measured extinction profiles, and measured (interval 3 only) and modeled relative humidity profiles are also shown for the purpose of this discussion.

[40] Interval 1 comprises the leading generation zone of the cirrostratus between 8 and 9 km. Nucleation of particles has just started, and so particles are still <~100 μm. Sedimentation of these small particles is not significant at this point, hence ambient and mean nucleation temperatures are almost identical, and the nucleation temperature distributions are narrow (3°C temperature range) and independent of particle size. Maximum supersaturation is 25% and the particle count is low, which is both the result of the gentle synoptic forcing that is applied and the chosen nucleation scheme and the associated parameters [*Meyers et al.*, 1992]. The simulation reproduces the cloud vertical extent well, but the synthetic cloud is about 400 m too low. We could have minimized this discrepancy by adjusting the tuning parameters, however, taking into account the overall agreement in all three intervals, the data shown are the best compromise.

[41] Interval 2 centers at about 2.75 h of cirrus observation/simulation (Figure 7). At 8.7 km (height level 1), an elevated particle count and a spectrum similar to the one of interval 1 indicate that particle nucleation continues in the cloud top layer, in fact until the end of the simulation after 7 h (compare Figure 8). Aside from this primary nucleation

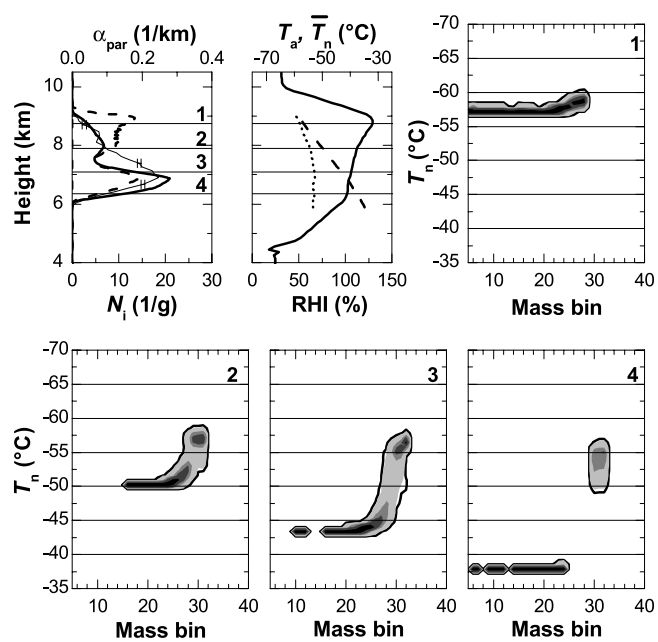

Figure 7. Similar to Figure 6 but for interval 2. As a cautionary note we stress that the relative T_n distribution is shown for each mass bin. Thus the figure does not allow one to judge what proportion of the overall particle numbers are small or large.

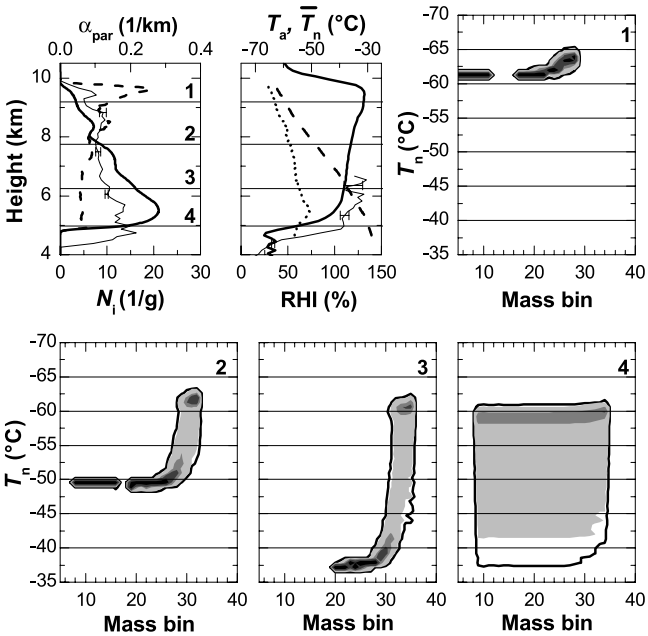

Figure 8. Similar to Figure 6 but for interval 3. The relative humidity profile as derived from the water vapor measurement with the GKSS Raman lidar and the temperature data of the radiosonde launch at Luleå is shown for comparison (thin solid curve with statistical error bars (Figure 8, top middle)).

zone, secondary nucleation zones exist at lower altitudes. As previously discussed by *Lin et al.* [2005], this is an effect of the low particle number concentration that leads to a growth-sedimentation-nucleation cycle. Particles sedimenting out of the top layer are too few in number to effectively limit relative humidity via growth and to compensate the increase in supersaturation in response to continuous forcing. Eventually, the critical supersaturation is reached and new particles form if ice nuclei are present (heterogeneous nucleation). The midcloud nucleation zones are visible in the nucleation temperature versus mass bin plots as small particle modes at relatively warm nucleation temperatures (at height levels 3 and 4 in interval 2, at height level 2 in interval 3). The large particle mode originates from particles that formed at colder temperatures and grew while sedimenting through the ice cloud. Because of the bimodal particle spectrum, mean nucleation temperature deviates increasingly from the ambient temperature with distance to cloud top. The cirrus geometry and the extinction profile are well reproduced by the microphysical model.

[42] The microphysical model results for interval 3 are shown in Figure 8. Particle number concentration is elevated above 8.3 km, below that height the cirrus consists of large (maximum dimensions exceeding 500 μm) but relatively few (4–7 g^{-1}) particles. Sublimation of ice particles is observed in subsaturated air near the cloud bottom (height level 4) as the mass distribution of particles with the same nucleation temperature widens to smaller particle masses. In-cloud relative humidity (RHI) increases with height because of the aforementioned only modest depletion of the water vapor reservoir, which results in a middle to upper portion of the cloud that is quite humid (RHI between 115% and 125%). RHI modeling is in qualitative agreement with the humidity profile obtained from the lidar water vapor measurement and the radiosonde temperature data if the differing base heights are taking into account.

[43] The cirrus cloud base is not reproduced well, the modeled base height is about 600 m too high. Our sensitivity tests show that by increasing the uplift from 2 to 5 cm/s and adjusting atmospheric humidity to slightly lower values (i.e., with the model settings used previously [*Reichardt et al.*, 2002a; *Kärcher*, 2005; *Lin et al.*, 2005]), modeled and measured cirrus base height could be brought into perfect agreement, but only at the expense of a poorer simulation of the cloud extinction profile. With the stronger uplift, modeled optical depth increases much faster over time than the measured optical depth until it is a factor of 3.6 larger in interval 3. With an uplift of 2 cm/s and a moister atmosphere, optical depth is still overestimated, but the effect is drastically reduced: modeled and measured optical depths deviate in intervals 1–3 by, respectively, 0%, 9%, and 54%, simulation errors we consider acceptable in view of the simplifying assumptions we made in our model about forcing in general. In summary, we were able to model the temporal evolution of either cloud height and vertical extent or optical depth very well, but not with a single set of tuning parameters. Balancing both requirements led us to select the weaker uplift and the moister humidity profile for this study.

4.3. Optical Model Scenarios

[44] To study the effects of particle shape, morphological complexity, and particle alignment on the simulated development of the particle optical properties, three different scenarios are considered.

4.3.1. Monocrystals in 3-D Orientation

[45] The ice particles are assumed to be single crystals of columnar or planar shape. Particle orientation is random. Model parameters are h_1 and h_2; the name convention for this series of tests is M3DX, where X is either m, T_a, or T_n (see equation (13), the defining equation of f_{pla}). The list of model parameters does not include b_{col} and b_{pla}. To limit the parameter space, they were determined prior to the optical model runs (as explained in section 4.4) and kept at the retrieved values regardless of the optical model scenario assumed.

4.3.2. Polycrystals in 3-D Orientation

[46] In this scenario the cirrus particles can be either monocrystals or crystal clusters. Particle orientation is random. As discussed in section 3.2, the number of basic crystals that form the polycrystals is modeled by function μ with parameters μ_0, p_1, and p_2 (equation (16)). Together with h_1 and h_2 the total number of model parameters would thus be five. Sensitivity tests show, however, that the assumption $p_2 = h_2$ does not affect the model results significantly, and so this simplification is applied to limit the dimensionality of the parameter space to four (h_1, h_2, μ_0, p_1). The name convention for this series of tests is P3DX.

4.3.3. Monocrystals in 3-D or 2-D Orientation

[47] In this model scenario the effect of particle horizontal alignment is investigated. The ice particles are not allowed

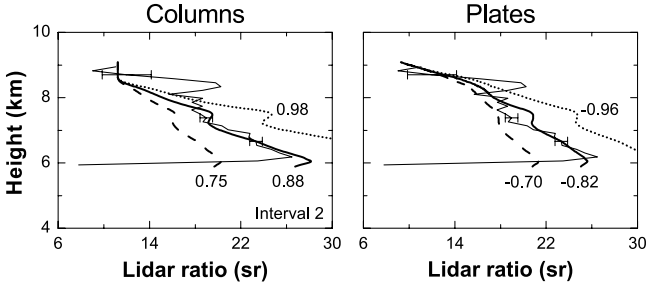

Figure 9. Observed (thin solid curve) and modeled lidar ratios (thick curves) for interval 2. It is assumed that the cirrus cloud consisted of only (left) hexagonal columns or (right) plates. Model results are shown for different values of b_{col} and b_{pla}, respectively. Error bars indicate statistical errors of the measurement.

to form polycrystals (μ_0 = 1). Furthermore, partial reduction in orientational freedom is not permitted ($e_{2D} \rightarrow 0$ in equation (15)), the wobble angle is either 0° (2-D orientation) or 90° (3-D orientation). Our sensitivity tests show that under this assumption it is sufficient to consider horizontal alignment of plate-like crystals alone, aligned columns are then irrelevant for the quality of the model results. This is likely due to the fact that the optical properties of perfectly aligned plates and columns are quite similar (see Figure 3, for both plates and columns $S_{par} < 6$ sr and $\delta_{par} \approx 0.04$ at $\omega_m = 0°$). The total number of model parameters is four (h_1, h_2, $c_{2D,pla}$, $d_{2D,pla}$), the notation is M2D3D*X*.

4.4. Retrieval of Parameters b_{col} and b_{pla}

[48] The two parameters b_{col} and b_{pla}, defining the functional dependence of particle aspect ratio on particle mass for columnar and planar particles respectively (see Table 1), are retrieved through coupled modeling of the measured lidar ratio profile in time interval 2. This interval is characterized by a monotonic dependence of the simulated particle mass on cloud height, cloud nucleation and ambient temperatures below −40°C (Figure 7), and by a simple structure of the measured optical properties (see, e.g., Figures 9 and 10). These facts combined suggest that the cirrus cloud in time interval 2 can best be described by a mixture of simple columnar and plate-like crystals (μ = 1), where the fraction of plate-like crystals decreases with height.

[49] We choose the parameters b_{col} and b_{pla} so that hexagonal columns and plates of equal mass have similar values of the lidar ratio. In this way, the lidar ratio depends mainly on the particle size, and thus on b_{col} and b_{pla}, whereas the particle depolarization ratio is defined mainly through the mixing ratio of columnar and plate-like crystals (this separation of variables simplifies the determination of optimum parameter sets in general). First we assume that cloud segment 2 consists of columnar hexagons only. An optimum b_{col} is retrieved by reproducing the experimental profile of the lidar ratio with the model (Figure 9). Then b_{pla} is obtained in a similar way, assuming the ice cloud contains only planar crystals.

[50] It is important to note that the retrieved optimum values of b_{col} and b_{pla}:

$$b_{col} = 0.88, \tag{17}$$

$$b_{pla} = -0.82, \tag{18}$$

fall within the observation range for columns reported by *Ono* [1969], *Auer and Veal* [1970], and *Mitchell and Arnott* [1994], or are close to the shape-length relationship for plates observed by *Auer and Veal* [1970], respectively (Figure 4). The agreement corroborates our assumptions made about the connection between the optical and microphysical properties of cirrus crystals, and increases confidence in the applicability of the theoretical optical data to cirrus measurements with lidar. All optical simulations that are presented in the following were performed while maintaining the b_{col} and b_{pla} values of equation (17) and equation (18).

4.5. Model Results

[51] Figure 10 compares the measured profiles of depolarization ratio and lidar ratio to those modeled under the assumption that the cirrus particles were monocrystals in random orientation (M3D scenario). Optimum model parameters were determined in an operator-assisted semi-automatized process (Table 2). A limited number of different sets of model parameters were chosen by the operator, and optical model runs were performed, to punctually probe the parameter space. From these the most promising parameter set was selected, and subsequently refined in additional series of simulations by applying the method of least squares.

[52] Only intervals 2 and 3 are shown because they are the most interesting. In interval 1 the simulated particle masses are so small and the temperatures so cold that in our model they are of columnar shape regardless of the scenario, and the aspect ratio and thus the optical properties of these small columns are largely insensitive to realistic sets of model parameters. Therefore no significant model variability is observed here. Modeled values for lidar ratio and depolarization ratio are, respectively, 11 sr and 52% which are within the ranges of the lidar measurement [*Reichardt et al.*, 2002c].

[53] Along with δ_{par} and S_{par}, the profiles of other key cloud properties are shown in Figure 10. In general, plate crystals abound more in the lower part of the cloud, and particle shape changes from thin plates and long columns to more compact hexagons with cloud height. This is particularly evident in the case of M3DT_a, for which the fraction of planar particles does not depend on cloud microphysics, whereas for M3DT_n and M3D*m* some exceptions exist. In the case of M3D*m*, interval 3, a decrease in f_{pla} and increasingly compact particles are observed toward the cloud bottom because of the sublimation of the ice crystals (see Figure 8). Furthermore, column mean aspect ratio dips around 5.5 km. At this height the particle mass distribution is narrow and close to the threshold value of 3.25 μg (Table 2), so the particle ensemble consists of mostly large planar particles (>70%) and a few small columns which tend to be isometric. In the case of M3DT_n, the fluctuations

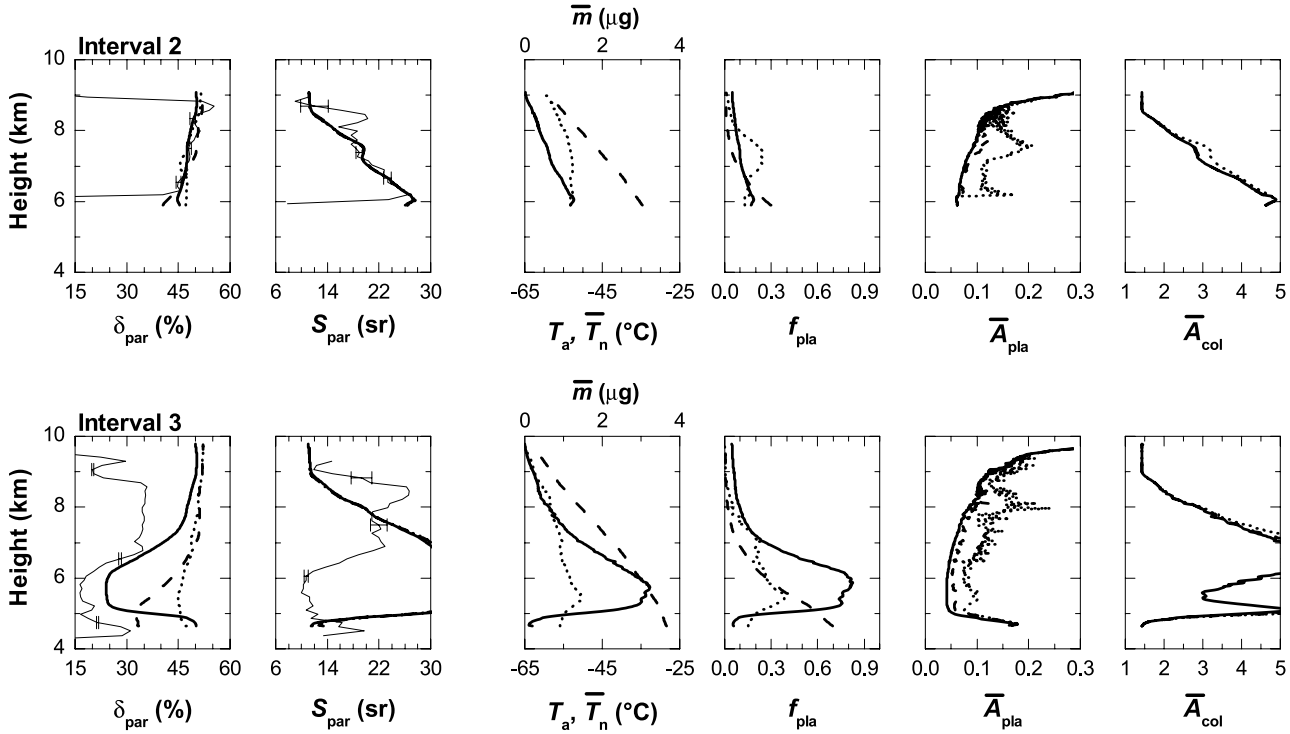

Figure 10. Model results obtained for monocrystals in 3-D orientation for (top) interval 2 and (bottom) interval 3. From left to right, modeled and observed particle depolarization ratio δ_{par} and lidar ratio S_{par}; mean particle mass $\overline{m}$, ambient temperature T_a, and mean nucleation temperature $\overline{T}_n$; fraction of planar particles f_{pla}; and mean aspect ratio of plates $\overline{A}_{pla}$ and columns $\overline{A}_{col}$. In the simulations it is assumed that the cloud properties depend on either particle mass m (solid curves), ambient temperature T_a (dashed curves), or nucleation temperature T_n (dotted curves). Thin solid curves show the lidar measurements (with error bars). Model results for interval 1 are nearly independent of the model scenario and agree well with the observations in all cases and are therefore not shown.

in $\overline{A}_{pla}$ mirror the (midcloud) nucleation layers. We discuss as an example the spike in $\overline{A}_{pla}$ at 7.9 km (interval 3) which corresponds with height level 2 in Figure 8. The newly nucleated small particles have nucleation temperatures close to the threshold temperature of −45°C and are therefore mostly planar in shape, which shifts the mass distribution of plates to smaller masses and thus to larger aspect ratios.

[54] The M3D simulations can reproduce both optical properties in interval 2, but fail to model the lower part of the cirrus cloud in interval 3. M3Dm and M3DT_a reproduce depolarization ratios better than M3DT_n, but not lidar ratios. The discrepancy is so pronounced that only unrealistic values of b_{col} and b_{pla} close to 0 would improve the results, at the expense of larger differences between modeled and measured lidar ratios in interval 2 and in the upper portion of the cirrus in interval 3. In summary, the assumption of randomly oriented monocrystals is insufficient to explain the cloud optical properties in this case study.

[55] The agreement in lidar ratio in interval 3 can be improved if polycrystals instead of monocrystals are assumed. Small crystals have smaller lidar ratios than large particles, and so an optical break up of a single crystal leads to the needed reduction in lidar ratio. The results for the polycrystal (P3D) simulations are presented in Figure 11. The optical properties of interval 3 are now better reproduced than in Figure 10, yet the agreement in lidar ratio in interval 2 is less perfect for model scenarios P3DT_a and P3DT_n. Furthermore, P3DT_n fails to reproduce the profiles

Table 2. Optimum Sets of Model Parameters for the Different Model Scenarios[a]

Scenario	h_1	h_2	μ_0	p_1	$c_{2D,pla}$	$d_{2D,pla}$
M3Dm	0.58 μg^{-1}	3.25 μg	–	–	–	–
M3DT_a	0.09°C^{-1}	−25°C	–	–	–	–
M3DT_n	0.17°C^{-1}	−45°C	–	–	–	–
P3Dm	0.58 μg^{-1}	3.25 μg	30	1.50 μg^{-1}	–	–
P3DT_a	0.40°C^{-1}	−35°C	20	0.40°C^{-1}	–	–
P3DT_n	0.17°C^{-1}	−35°C	10	0.50°C^{-1}	–	–
M2D3Dm	0.58 μg^{-1}	3.25 μg	–	–	0.005	385 μm
M2D3DT_a	0.05°C^{-1}	−15°C	–	–	0.01	385 μm
M2D3DT_n	0.17°C^{-1}	−35°C	–	–	0.17	300 μm

[a]In all cases, b_{pla} and b_{col} are −0.82 and 0.88, respectively.

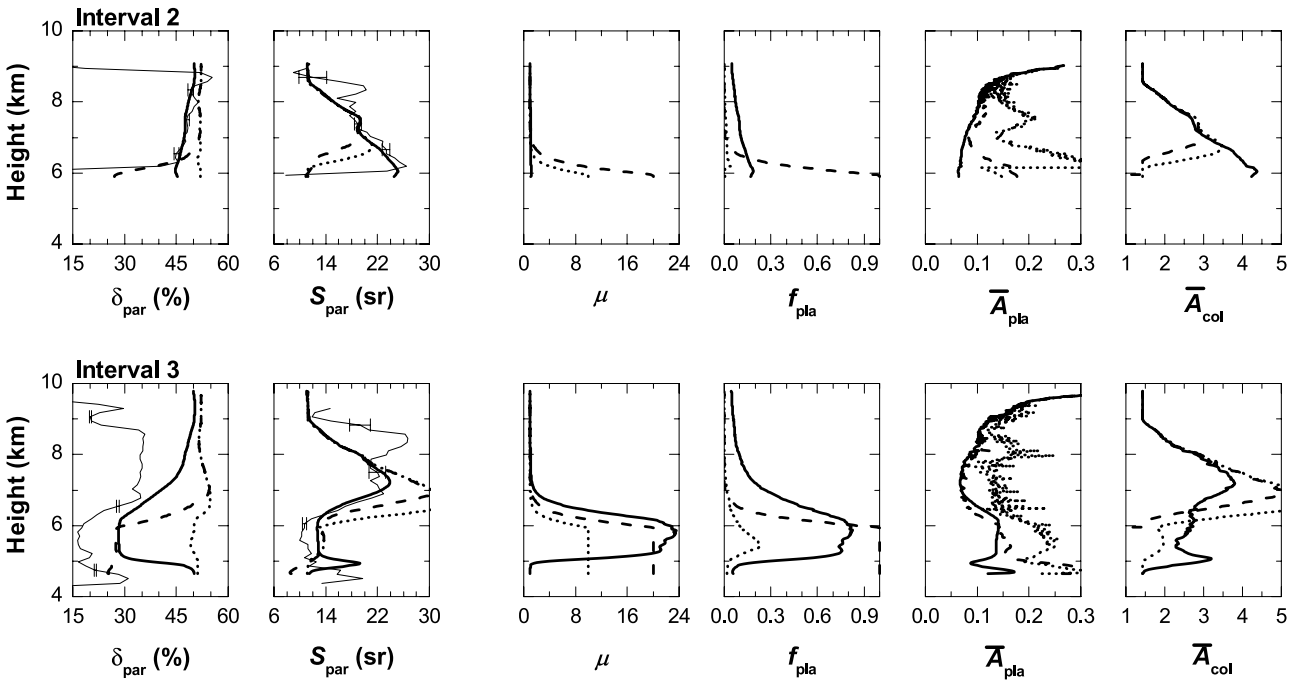

Figure 11. Similar to Figure 10 but for polycrystals in 3-D orientation. From left to right, modeled and observed particle depolarization ratio δ_{par} and lidar ratio S_{par}, number of basic crystals per particle μ, fraction of planar particles f_{pla}, and mean aspect ratio of plates $\overline{A}_{pla}$ and columns $\overline{A}_{col}$.

of the depolarization ratio in both intervals, so the important conclusion can be drawn that m and T_a (in this order) are the better parameters for splitting the ice mass into plate-like and column-like particles (particularly for depolarization ratio), which indicates that the ambient conditions affect the optical properties of atmospheric ice particles more than those conditions that prevailed when the particle formed. One has to note, however, that even P3Dm and P3DT_a cannot simulate the optical properties of the cloud top layer of the cirrostratus in interval 3, i.e., depolarization ratios of about >35% and lidar ratios >20 sr, which are, according to our theoretical optical data, the optical signature of crystal ensembles with extreme aspect ratios. Under our simple model assumptions this would require large particle masses at high altitudes, which the microphysical module does not generate.

[56] All model scenarios agree in that an abrupt transition from polycrystals to monocrystals at temperatures between −35 and −40°C is required to simulate the steep gradients in depolarization ratio and lidar ratio at 6.5 km. Interestingly, this temperature range is roughly the same as the midcloud temperatures (−39°C to −45°C) at which *Platt and Dilley* [1981] noted a change in their cirrus backscatter-to-extinction ratio data obtained at a continental midlatitude site, a change they attributed to a transition in particle morphology.

[57] In summary, model scenarios P3Dm and P3DT_a can both simulate the lidar observations well. According to the model, the cirrostratus consisted of polycrystalline particles with predominantly planar basic crystals in its bottom layer, and monocrystals above, with the fraction of columns increasing and the shape and size of the particles changing from relatively large thin plates and long columns to small, more isometric crystals from cloud center to top. This microphysical interpretation of the lidar measurements compares favorably with particle profiles sampled in situ [*Korolev et al.*, 1999; *Yang et al.*, 2001]. For example, *Korolev et al.* [1999] recorded particle habits with a cloud particle imager (CPI) in Arctic cirrus and stratiform clouds associated with frontal systems down to temperatures of −45°C, which overlaps with the temperature range of cirrus interval 3 below 7 km. They found that, on average, the ice particles were predominantly faceted polycrystalline particles consisting of combinations of different ice crystals habit (i.e., plates, columns) growing in different directions, sublimating ice particle clusters with smooth curving sides and edges, or particles that fall in an intermediate category. Faceted monocrystals (hexagonal columns and plates) were relatively rare, with their frequency of occurrence increasing with altitude (8% at around −45°C). Furthermore, the given examples of CPI images suggest that columns were more often found at colder temperatures (aspect ratios between one and three) and (thick) plates at warmer temperatures. In our case study, indeed polycrystals dominate ($\mu \gg 1$) below 7 km, f_{pla} decreases with height, and $\overline{A}_{col} < 3$ (Figure 11). As stated before, sublimating particles probably did not play a role except near the cloud bottom (Figure 8), so in our case study it is not necessary to consider scattering by particles with rounded parts. However, the results of *Korolev et al.* [1999] suggest that these particles may have to be taken into account in future cirrus modeling.

[58] It is also instructive to compare our modeled habit distribution to the particle shapes that *Whiteway et al.* [2004] found in cirrus clouds over Australia. During two aircraft campaigns, particle habits of midlatitude frontal cirrus and of outflow cirrus from deep tropical convection were obtained with a CPI. A second aircraft equipped with an elastic backscatter lidar served as a pathfinder. As an

interesting example of a midlatitude cirrus, *Whiteway et al.* [2004] present an ice cloud with a broad particle spectrum extending to the minimum resolution of the CPI (10 μm) that consisted of mostly irregular and columnar crystals throughout its vertical range. The irregular particles dominated in number, but showed the tendency of being smaller than the columns, which lead *Whiteway et al.* [2004] to assume that possibly the irregular particles were in an earlier phase of growth and had not yet developed a defined habit. In contrast, the maximum dimensions of the particles sampled in the outflow cirrus (and the remnants of the tropical storm) were without exception larger than 95 μm, and so particle habits were well developed. Mainly hexagonal plates, columns, and aggregates of hexagonal plates and columnar crystals (except for the very cloud top where many of the particles were bullet rosettes) were found, and the aggregates got smaller and less common with cloud height. These are exactly the particles that are represented in our optical-microphysical cirrus model, and so one can expect that it will perform well for this type of cirrus. This would certainly not be the case for the midlatitude cirrus of *Whiteway et al.* [2004] with the large numbers of small, irregular particles, however, it is worth remembering that it were habit profiles of (northern) midlatitude cirrus clouds sampled over the continental United States [*Heymsfield and Iaquinta*, 2000; *Miloshevich et al.*, 2001; *Yang et al.*, 2001] that guided us in designing our optical model module and where our model would probably work just fine. In summary, the discussion of the in situ habit measurements illustrates the limitations of our current model, and so the range of its applicability must be assessed very carefully.

[59] Our P3Dm and P3DT_a results are also in agreement with the laboratory studies of *Bailey and Hallett* [2004]. The authors investigated ice crystal growth characteristics under conditions comparable with those in the atmosphere and found that at temperatures between -20°C and -40°C and ice supersaturations >2% the most frequent habits observed were plate-like polycrystals and plates. Just below -40°C they reported a marked shift to columnar behavior for ice supersaturations in excess of 10%, the complexity of forms increasing with increasing supersaturation. For supersaturations in the range of 10% to 25%, which probably comes close to the conditions under which our cirrostratus developed (Figure 8), long solid columns and polycrystals with columnar and plate-like components were observed.

[60] The results of model runs with, in part, horizontally aligned ice plates (and randomly oriented columns) are highlighted in Figure 12. These M2D3D simulations yield results of similar quality like the P3D model, but this time a dependence of f_{pla} on T_a rather than on m is preferable. M2D3DT_n performs much better than P3DT_n and also reproduces the observations satisfactorily. As it has been stated before, aligned columns are not required in M2D3D runs. The critical particle size for horizontal alignment is the same for M2D3Dm and M2D3DT_a (385 μm) but considerably smaller for M2D3DT_n (300 μm), while the fraction of 2-D-oriented plates ($f_{2D,pla}$) increases by a factor of 34. These parameter adjustments counterbalance the differences in the number of plates available for alignment (f_{pla}) and the sizes of these plates (e.g., in interval 3 at 5.5 km, M2D3Dm generates 75% thin/large plates while M2D3DT_n models 20% thicker/smaller plates).

[61] Looking at the P3D and M2D3D profiles in Figures 11 and 12, it seems probable that a combination of the two scenarios would yield even better agreement between observation and simulation, at least in the case of an m-dependent parameterization of f_{pla} and μ, and it is likely indeed that the natural ice cloud contained both single crystals and crystal clusters, both in random or 2-D orientation. In such a combined scenario even a large threshold particle size $d_{2D,pla}$ similar to the one retrieved in the M2D3D scenarios (where it is difficult to interpret) would make sense, for it could be argued that the optically dominant basic crystal of polycrystals is not perfectly aligned horizontally if $<d_{2D,pla}$, and hence specular reflections are not observed. However, we refrained from doing so because we wanted to keep the model as straightforward and the parameter space as small as possible in order to avoid the perception that we overly model our data.

[62] In conclusion, good agreement between lidar and synthetic data is found for all optical properties and all measurement periods considered in this case study, except for the cirrus top layer in interval 3. In view of the simplifying assumptions made about the dynamical forcing (time- and height-independent updraft wind speed), and the optical model, the observed differences are generally remarkably small. These results support the proposed microphysical interpretation of cirrus measurements obtained with lidar [*Reichardt et al.*, 2002c].

5. Summary and Outlook

[63] A model is presented that permits the simulation of the optical properties of cirrus clouds as measured with depolarization Raman or high spectral resolution lidars. It comprises a one-dimensional cirrus model with explicit microphysics, and an optical module that transforms the microphysical model output to cloud and particle optical properties. The optical model takes into account scattering by planar and columnar monocrystals and polycrystals in random orientation or with reduced orientational freedom. Key cloud properties such as the fraction of plate-like particles and the number of basic crystals per polycrystal can be parameterized in terms of the ambient temperature, the nucleation temperature, or the mass of the particles.

[64] The optical-microphysical model is used to simulate the depolarization Raman lidar measurement of a synoptically forced Arctic cirrostratus in a first case study. It turns out that a cirrus cloud consisting of only monocrystals in random orientation is too simple a model scenario to explain the observations. However, good agreement between simulation and observation is reached when the formation of polycrystals or the horizontal alignment of monocrystals is permitted in the sensitivity tests. Only the moderately high depolarization ratios and high lidar ratios of one cloud top layer are not properly reproduced. Moreover, the model results show that the parameterization of the plate fraction and the morphological complexity is preferably done in terms of the particle mass, or ambient temperature rather than the nucleation temperature which indicates that the ambient conditions affect the optical properties of atmospheric ice particles more than those conditions that prevailed when the particle formed. Furthermore, the modeled height profiles of particle shape and size are in excellent

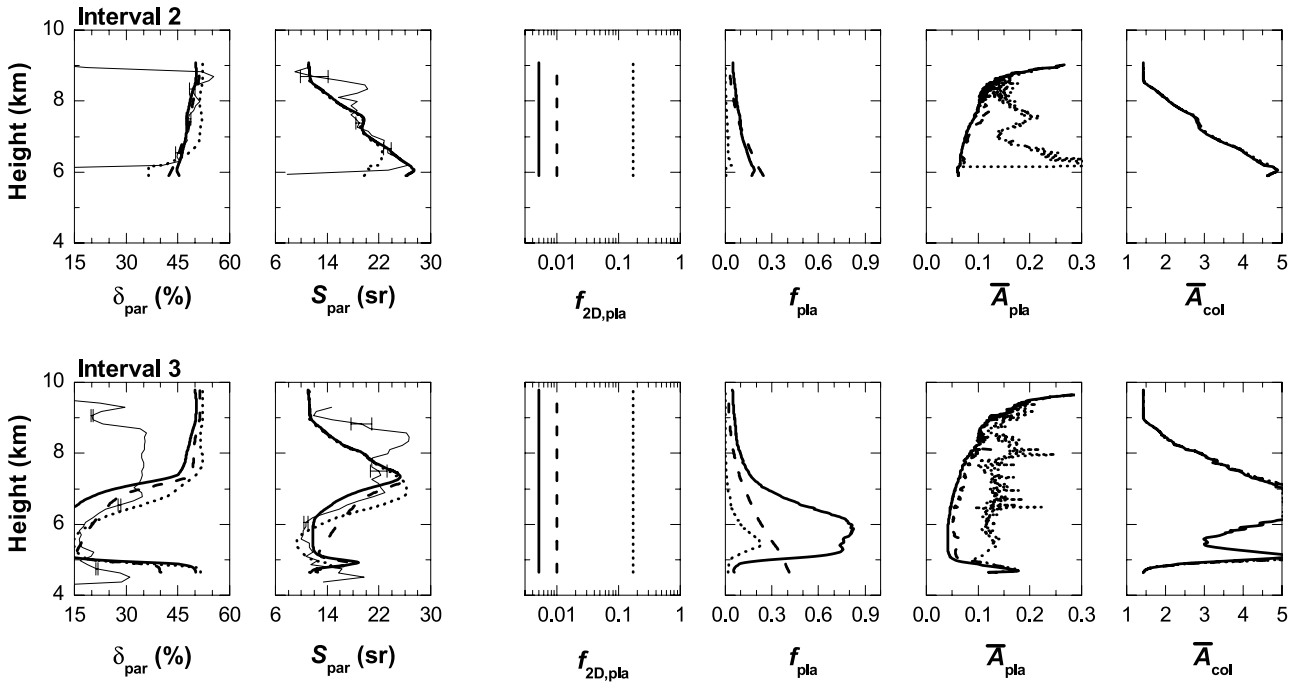

Figure 12. Similar to Figure 10 but for monocrystals in 3-D or 2-D orientation. From left to right, modeled and observed particle depolarization ratio δ_{par} and lidar ratio S_{par}, fraction of 2-D-oriented plates $f_{2D,pla}$, fraction of planar particles f_{pla}, and mean aspect ratio of plates $\overline{A}_{pla}$ and columns $\overline{A}_{col}$.

agreement with airborne particle sampling [*Yang et al.*, 2001] and laboratory studies of particle growth [*Bailey and Hallett*, 2004], i.e., (partly horizontally oriented) polycrystalline particles with predominantly planar basic crystals in the cloud bottom layer, and monocrystals above, with the fraction of columns increasing and the shape and size of the particles changing from relatively large thin plates and long columns to small, more isometric crystals from cloud center to top. The findings of this case study clearly corroborate the basic concept of the microphysical interpretation of cirrus measurements with lidar as suggested by *Reichardt et al.* [2002c].

[65] The encouraging results of this study warrant further investigations in the applicability of the optical-microphysical model. This is especially important because the cold Arctic frontal cirrus modeled here can certainly not be regarded as representative of ice clouds in general. Interesting test cases would include, e.g., frontal cirrus clouds at midlatitudes, and outflow cirrus from deep tropical convection. Preferably, cirrus observations should be analyzed for which lidar and in situ data exist. As the next step, however, we plan to perform cirrus measurements with a depolarization Raman lidar with Rayleigh/Raman integration method temperature measurement capability. This will allow us to compare modeled and measured [*Reichardt and Reichardt*, 2006] effective particle sizes.

Notation

Atmospheric and cloud bulk properties at a given height

$\overline{A}_{col}$, $\overline{A}_{pla}$ Mean aspect ratio of columns, plates.
$\overline{m}$ Mean particle mass.
N_i Number concentration of ice particles.
S_{par} Particle lidar ratio.
T_a Ambient temperature.
$\overline{T}_n$ Mean nucleation temperature.
α_{par} Volume extinction coefficient.
β_{par}, $\beta^{\parallel}_{par}$, $\beta^{\perp}_{par}$ Volume backscatter coefficient, in parallel polarization, in orthogonal polarization.
δ_{par} Particle depolarization ratio.

Properties of particles of a given mass and nucleation temperature at a given height

A Aspect ratio.
d Maximum dimension.
f Probability of having a certain shape and spatial orientation.
G Geometrical cross section.
m Mass.
n Number concentration.
p^{π} Value of scattering phase function at angle π.
T_n Nucleation temperature.
Δ Linear depolarization ratio at scattering angle π.
μ Number of crystal elements per particle cluster.
ω, ω_m Wobble angle, maximum wobble angle.
ϱ Ice density.

Model parameters

b_{col}, b_{pla} Parameter determining the functional dependence of A on d for columns, plates.
$c_{2D,col}$, $c_{2D,pla}$ Probability of horizontal alignment for columns > $d_{2D,col}$, plates > $d_{2D,pla}$ (parameter).

$d_{2D,col}$, $d_{2D,pla}$ Threshold size for horizontal alignment of columns, plates (parameter).

$e_{2D,col}$, $e_{2D,pla}$ Parameter determining the gradient of the decrease in orientational freedom with size for columns > $d_{2D,col}$, plates > $d_{2D,pla}$.

h_1, h_2 Parameters determining the fraction of plates.

p_1, p_2 Parameters determining the number of crystal elements per particle cluster (together with μ_0).

μ_0 Maximum number of crystal elements per particle cluster (parameter).

Models

M3D*X* Ice particles are single columns or plates in random orientation. Key cloud properties are functions of either ambient temperature ($X = T_a$), nucleation temperature ($X = T_n$), or mass ($X = m$).

P3D*X* Ice particles are clusters of columns or plates in random orientation.

M2D3D*X* Ice particles are single columns or plates in horizontal alignment or random orientation.

[66] **Acknowledgments.** This work was funded by the European Commission (grant ENV4-CT95-0162) and the German Bundesministerium für Bildung, Wissenschaft und Technologie (grant 01LO9504/5). We appreciate the support of Donald Anderson and Hal Maring of NASA's Radiation Sciences Program.

References

Ansmann, A., U. Wandinger, M. Riebesell, C. Weitkamp, and W. Michaelis (1992), Independent measurement of extinction and backscatter profiles in cirrus clouds by using a combined Raman elastic-backscatter lidar, *Appl. Opt.*, *31*, 7113–7131.

Auer, A. H., Jr., and D. L. Veal (1970), The dimension of ice crystals in natural clouds, *J. Atmos. Sci.*, *27*, 919–926.

Bailey, M., and J. Hallett (2004), Growth rates and habits of ice crystals between −20° and −70°C, *J. Atmos. Sci.*, *61*, 514–544.

Benedetti, A., and G. L. Stephens (2001), Characterization of errors in cirrus simulations from a cloud resolving model for application in ice water content retrievals, *Atmos. Res.*, *59–60*, 393–417.

Benedetti, A., G. L. Stephens, and J. M. Haynes (2003), Ice cloud microphysics retrievals from millimeter radar and visible optical depth using an estimation theory approach, *J. Geophys. Res.*, *108*(D11), 4335, doi:10.1029/2002JD002693.

Chen, J.-P., G. M. McFarquhar, A. J. Heymsfield, and V. Ramanathan (1997), A modeling and observational study of the detailed microphysical structure of tropical cirrus anvils, *J. Geophys. Res.*, *102*, 6637–6653.

Donovan, D. P., A. C. A. P. van Lammeren, R. J. Hogan, H. W. J. Russchenberg, A. Apituley, P. Francis, J. Testud, J. Pelon, M. Quante, and J. Goddard (2001), Cloud effective particle size and water content profile retrievals using combined lidar and radar observations: 2. Comparison with IR radiometer and in situ measurements of ice clouds, *J. Geophys. Res.*, *106*, 27,449–27,464.

Fouilloux, A., and J. Iaquinta (1998), Mesoscale cirrus cloud modeling and comparisons against experimental data collected on 17 April 1994 during the EUCREX campaign, *Mon. Weather Rev.*, *126*, 2422–2434.

Harrington, J. Y., and P. Q. Olsson (2001), A method for the parameterization of cloud optical properties in bulk and bin microphysical models. Implications for arctic cloudy boundary layers, *Atmos. Res.*, *57*, 51–80.

Hess, M., R. B. A. Koelemeijer, and P. Stammes (1998), Scattering matrices of imperfect hexagonal ice crystals, *J. Quant. Spectrosc. Radiat. Transfer*, *60*, 301–308.

Heymsfield, A. (1972), Ice crystal terminal velocities, *J. Atmos. Sci.*, *29*, 1348–1357.

Heymsfield, A. (1986), Ice particles observed in a cirriform cloud at −83°C and implications for polar stratospheric clouds, *J. Atmos. Sci.*, *43*, 851–855.

Heymsfield, A. J., and J. Iaquinta (2000), Cirrus crystal terminal velocities, *J. Atmos. Sci.*, *57*, 916–938.

Heymsfield, A. J., and C. M. R. Platt (1984), A parameterization of the particle size spectrum of ice clouds in terms of the ambient temperature and the ice water content, *J. Atmos. Sci.*, *41*, 846–855.

Iaquinta, J., H. Isaka, and P. Personne (1995), Scattering phase function of bullet rosette ice crystals, *J. Atmos. Sci.*, *52*, 1401–1413.

Intrieri, J. M., G. L. Stephens, W. L. Eberhard, and T. Uttal (1993), A method for determining cirrus cloud particle sizes using lidar and radar backscatter technique, *J. Appl. Meteorol.*, *32*, 1074–1082.

Jensen, E. J., O. B. Toon, D. L. Westphal, S. Kinne, and A. J. Heymsfield (1994), Microphysical modeling of cirrus: 1. Comparison with 1986 FIRE IFO measurements, *J. Geophys. Res.*, *99*, 10,421–10,442.

Kärcher, B. (2005), Supersaturation, dehydration, and denitrification in Arctic cirrus, *Atmos. Chem. Phys.*, *5*, 1757–1772.

Khvorostyanov, V. I., and K. Sassen (1998), Cirrus cloud simulation using explicit microphysics and radiation. Part I: Model description, *J. Atmos. Sci.*, *55*, 1808–1821.

Khvorostyanov, V. I., J. A. Curry, J. O. Pinto, M. Shupe, B. A. Baker, and K. Sassen (2001), Modeling with explicit spectral water and ice microphysics of a two-layer cloud system of altostratus and cirrus observed during the FIRE Arctic Clouds Experiment, *J. Geophys. Res.*, *106*, 15,099–15,112.

Khvorostyanov, V. I., J. A. Curry, I. Gultepe, and K. Strawbridge (2003), A springtime cloud over the Beaufort Sea polynya: Three-dimensional simulation with explicit spectral microphysics and comparison with observations, *J. Geophys. Res.*, *108*(D9), 4296, doi:10.1029/2001JD001489.

Klett, J. D. (1995), Orientation model for particles in turbulence, *J. Atmos. Sci.*, *52*, 2276–2285.

Korolev, A. V., G. A. Isaac, and J. Hallett (1999), Ice particle habits in Arctic clouds, *Geophys. Res. Lett.*, *26*, 1299–1302.

Lin, R.-F. (1997), A numerical study of the evolution of nocturnal cirrus by a two-dimensional model with explicit microphysics, Ph.D. thesis, 199 pp., Pa. State Univ., University Park.

Lin, R.-F., D. O. Starr, J. Reichardt, and P. J. DeMott (2005), Nucleation in synoptically forced cirrostratus, *J. Geophys. Res.*, *110*, D08208, doi:10.1029/2004JD005362.

Liu, H.-C., P. K. Wang, and R. E. Schlesinger (2003), A numerical study of cirrus clouds. Part I: Model description, *J. Atmos. Sci.*, *60*, 1075–1084.

Macke, A. (1993), Scattering of light by polyhedral ice crystals, *Appl. Opt.*, *32*, 2780–2788.

Macke, A., J. Mueller, and E. Raschke (1996), Single scattering properties of atmospheric ice crystals, *J. Atmos. Sci.*, *53*, 2813–2825.

Mason, B. J., G. W. Bryant, and A. P. van den Heuvel (1963), The growth habits and surface structure of ice crystals, *Philos. Mag.*, *8*, 505–526.

Meyers, M. P., P. J. DeMott, and W. R. Cotton (1992), New primary ice-nucleation parameterizations in an explicit cloud model, *J. Appl. Meteorol.*, *31*, 708–721.

Miloshevich, L. M., H. Vömel, A. Paukkunen, A. J. Heymsfield, and S. J. Oltmans (2001), Characterization and correction of relative humidity measurements from Vaisala RS80-A radiosondes at cold temperatures, *J. Atmos. Oceanic Technol.*, *18*, 135–156.

Mitchell, D. L. (1994), A model predicting the evolution of ice particle size spectra and radiative properties of cirrus clouds. Part I: Microphysics, *J. Atmos. Sci.*, *51*, 797–816.

Mitchell, D. L., and W. P. Arnott (1994), A model predicting the evolution of ice particle size spectra and radiative properties of cirrus clouds. Part II: Dependence of absorption and extinction on ice crystal morphology, *J. Atmos. Sci.*, *51*, 817–832.

Mitchell, D. L., S. K. Chai, Y. Liu, A. J. Heymsfield, and Y. Dong (1996a), Modeling cirrus clouds. Part I: Treatment of bimodal size spectra and case study analysis, *J. Atmos. Sci.*, *53*, 2952–2966.

Mitchell, D. L., A. Macke, and Y. Liu (1996b), Modeling cirrus clouds. Part II: Treatment of radiative properties, *J. Atmos. Sci.*, *53*, 2967–2988.

Ono, A. (1969), The shape and riming properties of ice crystals in natural clouds, *J. Atmos. Sci.*, *26*, 138–147.

Platt, C. M. R., and A. C. Dilley (1981), Remote sensing of high clouds. IV: Observed temperature variations in cirrus optical properties, *J. Atmos. Sci.*, *38*, 1069–1082.

Platt, C. M. R., N. L. Abshire, and G. T. McNice (1978), Some microphysical properties of an ice cloud from lidar observation of horizontally oriented crystals, *J. Appl. Meteorol.*, *17*, 1220–1224.

Reichardt, J. (1999), Optical and geometrical properties of northern mid-latitude cirrus clouds observed with a UV Raman lidar, *Phys. Chem. Earth B*, *24*, 255–260.

Reichardt, J., and S. Reichardt (2006), Determination of cloud effective particle size from the multiple-scattering effect on lidar integration-method temperature measurements, *Appl. Opt.*, *45*, 2796–2804.

Reichardt, J., U. Wandinger, M. Serwazi, and C. Weitkamp (1996), Combined Raman lidar for aerosol, ozone, and moisture measurements, *Opt. Eng.*, *35*, 1457–1465.

Reichardt, J., R.-F. Lin, S. Reichardt, T. J. McGee, and D. O. Starr (2002a), Microphysical interpretation of cirrus measurements with lidar—Comparison to a coupled optical-microphysical model, paper presented at 11th Conference on Atmospheric Radiation, Am. Meteorol. Soc., Ogden, Utah.

Reichardt, J., S. Reichardt, A. Behrendt, and T. J. McGee (2002b), Correlations among the optical properties of cirrus-cloud particles: Implications for spaceborne remote sensing, *Geophys. Res. Lett.*, *29*(14), 1668, doi:10.1029/2002GL014836.

Reichardt, J., S. Reichardt, M. Hess, and T. J. McGee (2002c), Correlations among the optical properties of cirrus-cloud particles: Microphysical interpretation, *J. Geophys. Res.*, *107*(D21), 4562, doi:10.1029/2002JD002589.

Reichardt, J., S. Reichardt, P. Yang, and T. J. McGee (2002d), Retrieval of polar stratospheric cloud microphysical properties from lidar measurements: Dependence on particle shape assumptions, *J. Geophys. Res.*, *107*(D20), 8282, doi:10.1029/2001JD001021.

Reichardt, J., A. Dörnbrack, S. Reichardt, P. Yang, and T. J. McGee (2004), Mountain wave PSC dynamics and microphysics from ground-based lidar measurements and meteorological modeling, *Atmos. Chem. Phys.*, *4*, 1149–1165.

Sassen, K. (1980), Remote sensing of planar ice crystal fall attitudes, *J. Meteorol. Soc. Jpn.*, *58*, 422–429.

Sassen, K., and S. Benson (2001), A midlatitude cirrus cloud climatology from the Facility for Atmospheric Remote Sensing. Part II: Microphysical properties derived from lidar depolarization, *J. Atmos. Sci.*, *58*, 2103–2112.

Sassen, K., Z. Wang, V. I. Khvorostyanov, G. L. Stephens, and A. Bennedetti (2002), Cirrus cloud ice water content radar algorithm evaluation using an explicit cloud microphysical model, *J. Appl. Meteorol.*, *41*, 620–628.

Seifert, M., J. Ström, R. Krejci, A. Minikin, A. Petzold, J.-F. Gayet, U. Schumann, and J. Ovarlez (2003), In-situ observations of aerosol particles remaining from evaporated cirrus crystals: Comparing clean and polluted air masses, *Atmos. Chem. Phys.*, *3*, 1037–1049.

Westphal, D. L., et al. (1996), Initialization and validation of a simulation of cirrus using FIRE-II data, *J. Atmos. Sci.*, *53*, 3397–3429.

Whiteway, J., et al. (2004), Anatomy of cirrus clouds: Results from the Emerald airborne campaigns, *Geophys. Res. Lett.*, *31*, L24102, doi:10.1029/2004GL021201.

Yang, P., and K. N. Liou (1998), Single-scattering properties of complex ice crystals in terrestrial atmosphere, *Contrib. Atmos. Phys.*, *71*, 223–248.

Yang, P., B.-C. Gao, B. A. Baum, W. J. Wiscombe, Y. X. Hu, S. L. Nasiri, P. F. Soulen, A. J. Heymsfield, G. M. McFarquhar, and L. M. Miloshevich (2001), Sensitivity of cirrus bidirectional reflectance to vertical inhomogeneity of ice crystal habits and size distributions for two Moderate-Resolution Imaging Spectroradiometer (MODIS) bands, *J. Geophys. Res.*, *106*, 17,267–17,291.

Yang, P., Y. X. Hu, D. M. Winker, J. Zhao, C. A. Hostetler, L. Poole, B. A. Baum, M. I. Mishchenko, and J. Reichardt (2003), Enhanced lidar backscattering by quasi-horizontally oriented ice crystal plates in cirrus clouds, *J. Quant. Spectrosc. Radiat. Transfer*, *79–80*, 1139–1157.

M. Hess, Remote Sensing Technology Institute, German Aerospace Center, D-82234 Wessling, Germany. (michael.hess@dlr.de)

R.-F. Lin and D. O. Starr, Mesoscale Atmospheric Processes Branch, Laboratory for Atmospheres, NASA Goddard Space Flight Center, Greenbelt, MD 20771, USA. (lin@agnes.gsfc.nasa.gov; starr@agnes.gsfc.nasa.gov)

T. J. McGee, Atmospheric Chemistry and Dynamics Branch, Laboratory for Atmospheres, NASA Goddard Space Flight Center, Greenbelt, MD 20771, USA. (mcgee@aeolus.gsfc.nasa.gov)

J. Reichardt, Meteorologisches Observatorium Lindenberg, Deutscher Wetterdienst, Am Observatorium 12, D-15848 Tauche, Germany. (jens.reichardt@dwd.de)

S. Reichardt, Joint Center for Earth Systems Technology, University of Maryland, Baltimore County, Suite 320, 5523 Research Park Drive, Baltimore, MD 21228, USA. (sreichardt@aeolus.gsfc.nasa.gov)